Photostimulated desorption of CO from geologic calcite following 193-nm irradiation

Kenneth M. Beck, David P. Taylor, and Wayne P. Hess*
Environmental Molecular Sciences Laboratory, Pacific Northwest National Laboratory, Richland, Washington 99352
(Received 4 November 1996)

We report the results of a photostimulated desorption study of neutral CO product from geologic calcite using very low fluence 193-nm excimer laser radiation. Detailed product state distributions are obtained using $(2+1)$ resonance enhanced multiphoton ionization. The CO translational energy can be characterized by a temperature ($T=110\pm15$ K) significantly lower than that of the substrate ($T=295$ K). The CO rotational state distribution is non-Boltzmann and there is step structure every four or five rotational states. The evolution of CO emission as a function of laser exposure shows no incubation period or enhanced CO photodesorption over time. The CO yield is linear with laser power and displays no detectable threshold. The low kinetic energy of the desorbed CO and the nonthermal CO distributions implicate the decay of a surface species or state. [S0163-1829(97)00119-7]

INTRODUCTION

Calcium carbonate ($CaCO_3$) is an environmentally significant mineral that exists in several forms including orthorhombic aragonite, rhombohedral dolomite, and rhombohedral calcite. The carbonates, as a group, make up more than 10% of the Earth's sedimentary mass,[1] and calcite itself is present in the soil to the extent that it influences subsurface transport of heavy metals through interactions with ground water. The origins of calcite vary from geologically produced crystals, through biologically produced coral, to fossils such as Jurassic red tide. Many organisms secrete calcium carbonate to form exoskeletal structures. Calcium carbonate is also a component in the protective caliche layer below the waste storage tanks at the Hanford nuclear reservation. Our immediate interest in calcium carbonate, and molecular ionic compounds in general, arises from the need to perform microsample chemical analysis of mixed (radionuclides+chemical) hazardous wastes. Laser ablation mass spectrometry (LAMS) is an analytical technique being developed for this purpose. The LAMS technique has been successfully applied to complex solid and doped glass samples for quantitative elemental analysis.[2] But for a LAMS analysis to be effective here, desorption properties of these molecular ionic components must be understood.[3]

The mechanisms by which laser radiation interacts with solid samples during laser ablation are intensity dependent. These include linear absorption, thermal and optical runaway, and electron-neutral and electron-ion inverse bremsstrahlung.[4] Under conditions of high power density the final products may be heavily influenced by the chemical processes occurring in the laser-induced ablation plasma at or near the surface. After vaporization, subsequent chemistry involving electrons, ions, and neutral molecules can alter the composition of the analyte plume. These secondary reactions may be controlled and the nascent product state distribution accurately analyzed if the number density of desorbed species is sufficiently low. This is most readily accomplished by operating in a regime of low laser intensity and ultrahigh vacuum (UHV).

A detailed description of the photochemistry is less crucial when LAMS is used solely as a tool for elemental analysis. However, it is critically important to understand the chemistry of the ablation process if LAMS is to be used as a diagnostic tool for determining the chemical (molecular) composition and structure of the original material. In the present work, we restrict ourselves to a ''very low'' fluence regime using irradiances $<3\times10^5$ W/cm^2. Experiments using extremely low fluences are possible due to the efficiency of UV photostimulated desorption (PSD) and the sensitivity of laser ionization detection techniques under UHV conditions. At these low fluences the emitted particle number density is sufficiently low for the molecules to disperse without collisions allowing for the determination of nascent product state distributions of the desorbed molecules.

PSD of many simple ionic crystals has been reported by several groups, with alkyl halides receiving particular attention.[5–7] There has been much discussion of the nature of the excitation and desorption mechanisms.[8–11] Laser ablation studies of alkaline-earth ionic crystals have probed the excitation mechanism and the dynamics of neutral and ionic product formation.[12–14] There has also been extensive study of alkyl halide sputtering by the related technique of electron stimulated desorption.[6,7,15–21] Recent work[3,22–24] has been conducted on molecular ionic crystals: these materials are interesting because they exhibit strong ''molecular'' and charge-transfer absorptions in the UV region.

Calcite is a wide-band-gap, insulating material that possesses a strong characteristic optical absorption at wavelengths <214 nm. Recent reflection electron-energy-loss spectroscopy measurements have associated this absorption with the onset of the band gap ($E_g=6.0\pm0.35$ eV) and associate a small loss feature just above 5 eV with a surface state.[25] High-resolution x-ray photoelectron spectroscopy valence-band spectra of single-crystal calcite have recorded four prominent features. Comparison with initial *ab initio* density of states calculations showed good agreement and seems to indicate that the highest occupied valence orbitals are dominated by O $2p$ character (72%) with some mixing from Ca $4p$ (2%).[26] However, very recent work indicates that the conduction band may be seen as the site of substan-

tial ''mixing'' between O $2p$ and C $2p$ with Ca $4s$ atomic orbitals.[27]

Crystalline calcium carbonate is isostructural with sodium nitrate and the corresponding molecular ions are isoelectronic. However, calcite is a much more stable crystal than sodium nitrate; the melting point of sodium nitrate is only 308 °C while calcium carbonate melts at 1339 °C, with the first structural phase transition from aragonite to calcite occurring near 520 °C. In addition, natural calcite contains small and varying amounts of ionic impurities (e.g., Mn^{2+}, Pb^{2+}, Mg^{2+}) which tend to replace Ca^{2+}, or lie within vacant interstitial positions, within the crystal lattice.[28] The concentrations of impurities depend both upon the chemical (biogenic or geologic) and the geographical origins of the crystal. Pure, synthetic crystals have not been produced with a diameter greater than 10 μm. The dynamics of crystal growth are not well understood, but it is believed that the crystalline plane may be stabilized by impurity ions.[28]

In this paper we focus on laser desorption following a 6.42-eV (193-nm) excitation of calcite, analogous to similar studies conducted in this laboratory on $NaNO_3$.[3] There, both 213- and 266-nm radiation were used to excite resonantly and nonresonantly, respectively, the nitrate ion ($\pi^* \leftarrow \pi_2$) transition leading to the molecular desorption of NO from the surface. We examine laser/solid interactions following the excitation of single-crystal calcium carbonate by measuring the translational, rotational, and vibrational energy distributions of desorbed CO.

EXPERIMENT

The experimental procedure for obtaining state distributions from a laser desorbed species has been described previously.[3] Briefly, the experimental apparatus consists of a liquid-nitrogen-trapped diffusion pumped UHV chamber (base pressure 3×10^{-10} torr) equipped with a laser tier with laser access ports, and quadrupole (QMS's) and time-of-flight (TOF) mass spectrometers. Desorbed neutral species may be ionized by a second laser, for TOF detection, or by electron impact (70 eV) for QMS detection. The sample holder is mounted vertically on an x, y, z micrometer stage to access the electron spectrometers and the laser tier. The sample manipulator also has the capability to rotate the sample about the z axis and may be cooled to near liquid-nitrogen temperatures (90 K) and includes a button heater and thermocouples pressure mounted to the crystal sample for heating and monitoring.

Geologic samples of calcium carbonate (calcite form) are described by a hexagonal lattice (space group 167, $R3c$) with a rhombohedral primitive cell; the symmetry of the carbonate anion is D_{3d}. Large crystals of optical grade Iceland Spar used for these experiments are of Mexican and Chinese geologic origin which typically show an Mn^{2+} impurity abundance of $\sim$0.0008%. These crystals are cleaved in air along the 1014 crystal plane of the hexagonal lattice, structurally placing one oxygen, per carbonate group, out of plane. The resulting calcite chips are immediately mounted on the sample manipulator and introduced to UHV. Atomic force microscopy of cleaved calcite samples display wide flat crystal planes interrupted by single layer pits or steps separated by a few micrometers. Deeper pits, of several layers in depth, occur less frequently with a minimum surface density of 10^3 cm^{-2}.[29] Prior to irradiation, the calcite sample is heated *in vacuo* to 450 °C for 12 h to reduce surface contamination. It should also be noted that while most data are recorded at room temperature after cooling, a CO spectrum is observed for each new sample at 450 °C, where there should be minimal water vapor and hydrocarbon contamination. CO itself does not adsorb to insulators and insulating oxides at temperature above 100 K.[30]

The $CaCO_3$ crystals are irradiated with 5-ns pulses of 193-nm excimer laser emission (100 $\mu J/cm^2$) incident on the sample at 50° normal to the crystal face. The single crystal emits an orange luminescence at the point of irradiation that we use to orient and center the sample within the excitation beam. For the detection of CO we have chosen a sensitive method utilized by numerous researchers; $(2+1)$ resonance enhanced multiphoton ionization (REMPI).[31–35] The $(2+1)$ process involves two-photon excitation of the $B^1\Sigma \leftarrow\leftarrow X^1\Sigma$ transition followed by one-photon ionization from the B state to the ion ground electronic state. This is done with a second, tunable laser. The $(2+1)$ spectrum is characterized by a strong Q band obtained over a narrow frequency range $\sim$20 cm^{-1}. The subsequent analysis of the Q branch then affords insight into the rotational product state distribution.[36]

The probe-laser system consists of a Nd:YAG-pumped dye laser (YAG represents yttrium aluminum garnet) whose output is frequency doubled using a β-BBO crystal to produce tunable output that covers the 230-nm spectral region necessary for the $(2+1)$ REMPI detection of $v=1$ and 0 states of neutral CO. The doubled dye laser beam subsequently passes through a 1-mm aperature near the chamber and is focused ($f=20$ cm) to an estimated beam waist of $\sim$15 μm and a waist length of $\sim$2.9 mm. The nominal frequency bandwidth of the dye laser fundamental is 0.06 cm^{-1}. By translating the crystal towards the probe-laser beam the exact position and orientation of the probe with respect to the sample face is determined and adjusted by observing the microablation caused by the focused probe beam as it grazes the crystal edge. The crystal sample is then moved away so that the probe laser lies 2.5 mm above the crystal surface. The alignment of both the desorption and probe lasers and the optics is checked using HeNe lasers ($\lambda=632.8$ nm) aligned colinearly with each beam. The probe laser is then optimally delayed by 7–20 μs from the excitation pulse depending on sample temperature. The REMPI probe-laser and 193-nm pump-laser intensities were continuously monitored by photodiodes.

The positive ions produced in the REMPI process are detected using a Wiley-McClaren-type TOF mass spectrometer with a resolution of $\Delta m/m=150$ at $m/z=28$. The relative ion yields are measured using a boxcar integrator. TOF ion signals are captured on a digital scope and stored on a personal computer. We measure state population distributions using probe-laser powers of <35 μJ/pulse, or an estimated irradiance $<2\times10^5$ W/cm^2. We correct the measured rotational spectra for fluctuations in the laser power.[36] Velocity measurements of neutral CO are taken with laser delays stepped in 100–200-ns increments and averaged over 10 shots. To test the suitability of our $(2+1)$ REMPI technique

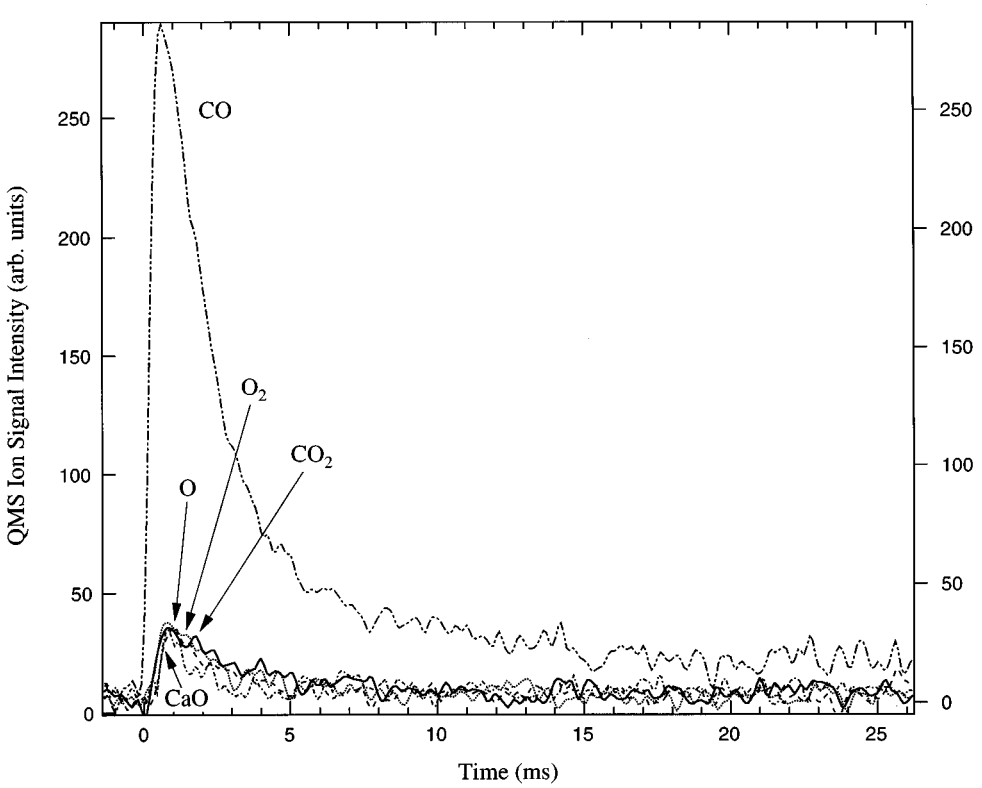

FIG. 1. QMS ion signals of neutral products desorbed from 193-nm irradiation of geologic calcite: CO (-···), O (---), O_2 (···), CO_2 (—), CaO (-·-). Ions of the neutral products are formed following 70-eV electron bombardment. Corrections to the recorded signals have been made for the CO fragmentation pattern (CO, 100%; O, 6.1%; C, 10%).

for determining products state distributions, we obtained and analyzed REMPI spectra from gas-phase samples of room-temperature CO under similar chamber and probe-laser conditions used for desorption studies of $CaCO_3$. The CO samples were admitted through a pulsed valve configured to provide a small leak at a CO sample pressure of $\sim 3 \times 10^{-8}$ torr. Well-resolved spectra of CO are obtained which can be well fit to a simulated Boltzmann distribution ($T = 295 \pm 10$ K).

RESULTS

At very low excitation laser fluences, the principal neutral desorption product from calcite is CO. Figure 1 displays the QMS signal of neutral species desorbed from calcite when irradiated with ~ 100 μJ/cm^2 of 193-nm radiation. CO dominates other constituents by an order of magnitude. Yet, even after accounting for ''cracking'' within the electron-impact ionizer, distinct signals for CaO, O, CO_2, and O_2 are apparent. At these low pump-laser fluences, the TOF-MS detects no CO cation or other ion signal. It is interesting that any CaO is desorbed at such low fluences; however the signal at $m/z = 56$ is well separated from other products, making it quite distinguishable in the QMS.

We conducted power dependence studies of the desorption process at fluences up to ~ 0.6 mJ/cm^2. CO was detected following electron-impact ionization using the quadrupole mass spectrometer. Figure 2 shows a double-logarithmic plot of the QMS signal versus pump-laser fluence. The slope of this line is 0.95 ± 0.1 and no observable threshold is detected. Additionally, shot-to-shot variations of pump-laser intensity are mimicked with proportional rises in the CO^+ signal. Together, these facts strongly suggest that a single-photon absorption process leads to molecular desorption of CO from calcite.

Initially, CO emission as a function of laser exposure is relatively large, but irreversibly decreases to a lower, steady-state value after days of exposure to 193-nm radiation. No dramatic growth in CO desorption products occurs after repeated irradiation, unlike nonresonant excitation of sodium nitrate at 248 (Ref. 37) and 266 nm.[3] An increase in desorption yield following an incubation period is often regarded as indicating that photostimulated desorption depends on the build up of additional surface defect sites. Its absence might be taken to infer that defect-driven desorption mechanisms, from photoproduced defect sites, do not play a dominant role.[38]

Figure 3 displays a low-resolution $(2+1)$ REMPI spectrum of desorbed CO which is showing both the (0-0) and (1-1) transitions. Approximately 6% of the desorbed CO contains a single quantum of vibrational energy (2140 cm^{-1}). Investigation of higher vibrational levels of a $B^1\Sigma$ state CO is hampered by the fact that their rate of predissociation is larger than for ionization. A study of CO photodesorbed from calcite using 213-nm excitation also found $>4\%$ of CO in $v = 1$. A two-point Boltzmann distribution with a 6% $v = 1$ vibrational population yields a temperature of 1100 K. In contrast, we find the CO velocity distribution to be quite slow and well characterized by a temperature well below that of the substrate.

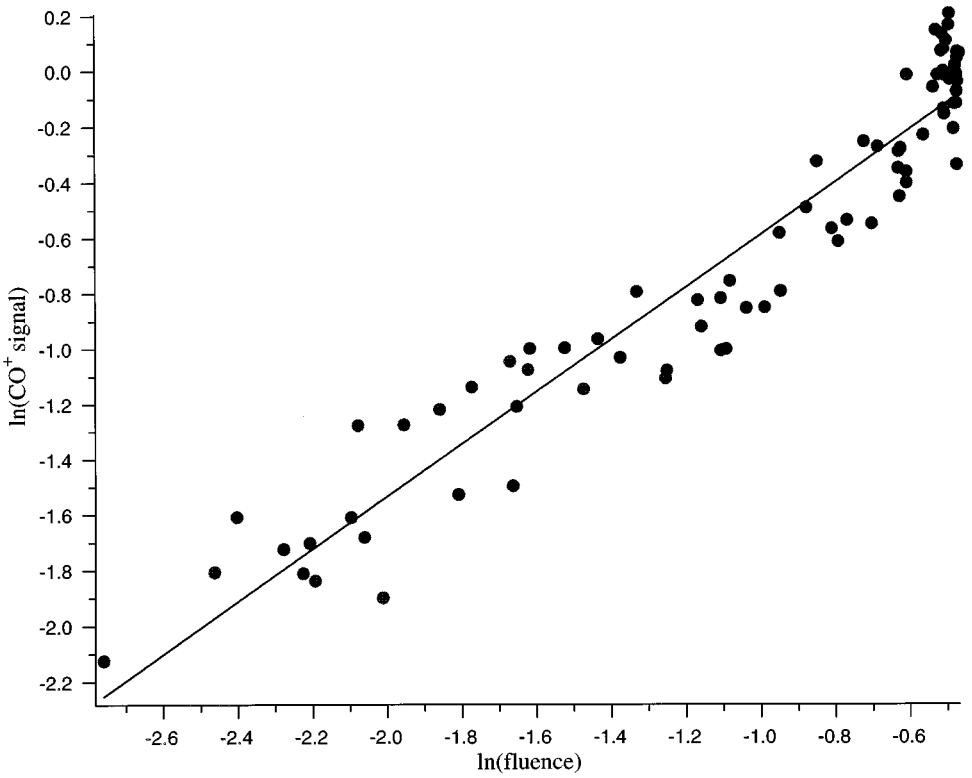

FIG. 2. Single-photon power dependence of CO neutral signal. A ln-ln plot of the QMS CO^+ ion signal versus the 193-nm laser fluence is displayed. Fluence ranges from 60 to 600 μJ/cm^2. A linear least-squares fit yields a slope$=0.95\pm0.1$. In addition, shot-to-shot variations in pump-laser power are observed to mimic the CO^+ signal.

Figure 4 represents the velocity distributions of desorbed CO for $Q(J)=5$ at a substrate temperature of 295 K for $v=0$ and 1. The TOF spectra are fit to a half-range Maxwell-Boltzmann velocity distribution function,[39] $P(t)$,

$$P(t)=\alpha x t^{-4}\exp\left[\frac{-\beta^2(x-\mu t)^2}{t^2}\right],$$

where x is the distance from the sample to the probe beam, t is the time difference between the two laser pulses, α is a proportionality constant, and the fitted parameters μ and β^2 are the flow velocity and $m/2kT$, respectively. The TOF spectra for $v=0$ can be fit with a translational temperature, $T_{\rm trans}=110\pm15$ K. Those for $v=1$ can be fit for $T_{\rm trans}=125\pm15$ K. These differences are within statistical error (one standard deviation) and show that there is little vibrational dependence to the velocity distributions of desorbed CO. In Fig. 4(c), the velocity distribution for $Q(J)=5$ in $v=0$ is displayed for a substrate temperature of 90 K. The fitted temperature of CO products is $T_{\rm trans}=20\pm10$ K.

In fitting the data, the flow velocity parameter is allowed to vary and is found to relax always to zero. A flow velocity of zero indicates a low probability of collisions in the desorption plume and places an upper bound on the desorption yield of <0.1 ML/laser pulse.[40] An approximate material removal rate may be estimated through comparison of the TOF signal intensities obtained from CO desorbed from calcite and those obtained from the gas sample (3×10^{-8} torr). With the assumptions of a calcite surface density of $\sim6\times10^{14}$ molecules/cm^2 ($\sigma_{\rm calcite}=2.71$ g/cm^3) and a plume volume of 0.014 cm^3 (at the instant the plume is probed), we estimate that less than 0.01% of a monolayer is removed per laser pulse. This corresponds to a desorption probability (average number of molecules desorbed per photon absorbed) of $<6\times10^{-4}$.

Figure 5 displays the resolved Q branch for the CO (0,0) $B^1\Sigma\leftarrow\leftarrow X^1\Sigma$ and (1,1) $B^1\Sigma\leftarrow\leftarrow X^1\Sigma$ transitions obtained following PSD from room-temperature $CaCO_3$. The appearance of Q-band structure is not unexpected since the difference between the X state ($v=0$, $B=1.931$ cm^{-1}) (Ref. 41) and B state ($v=0$, $B=1.948$ cm^{-1}) (Ref. 42) rotational constants causes a splitting of Q-branch transitions that increases with J. This splitting is greater than the combined Doppler and laser bandwidths for $Q(J)>7$ and approaches 1.0 cm^{-1} for $Q(J)=20$. Superimposed upon these scans are spectra simulating a thermal distribution at 295 K for CO rotational states up to the $Q(J)=23$.[36]

The rotational spectra of CO products—in contrast to the translational energy—appears similar to a thermal simulation done at the substrate temperature of 295 K. However, a nonthermal component is also revealed in the rotational spectra. Specifically, the spectrum for $v=0$ [Fig. 5(a)] even appears ''structurally'' nonthermal. A stepwise effect may be seen with population variations every 4–5 rotational levels; below thermal at low $Q(J)$, above thermal at mid $Q(J)$, and again below thermal at higher $Q(J)$. These effects in $v=0$ are repeatable for each calcite sample, and between samples of different origin. Similar effects in $v=1$ are difficult to observe in Doppler-limited spectra, because the entire Q branch

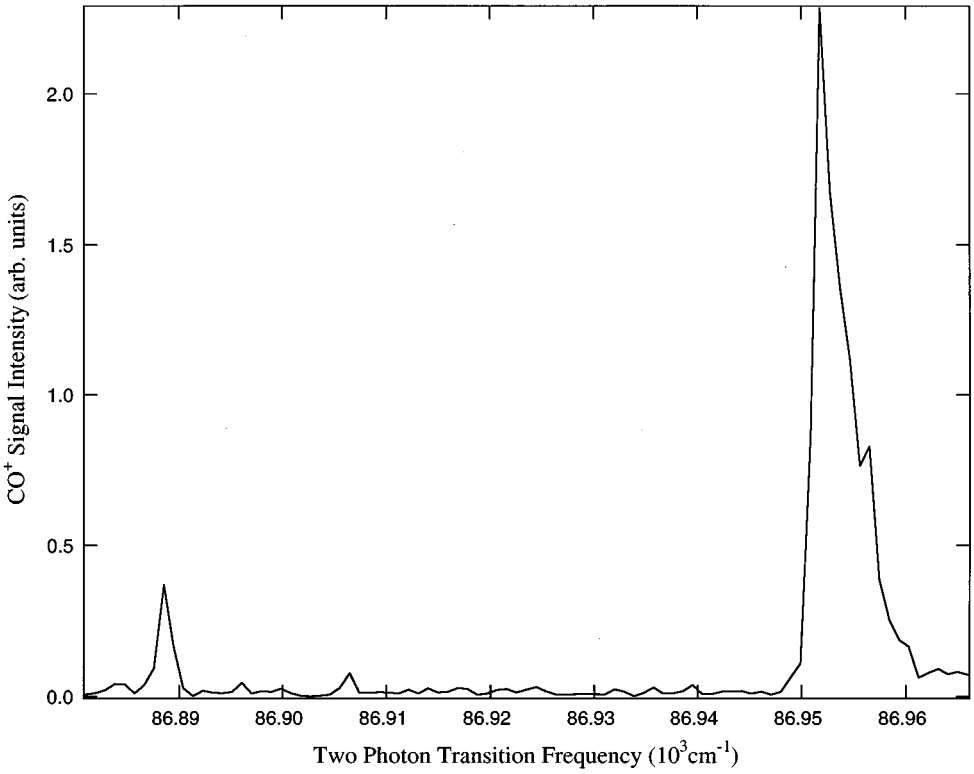

FIG. 3. Low-resolution vibrational energy distribution spectrum of CO products. Probed levels include only the (0,0) $B^1\Sigma \leftarrow\leftarrow X^1\Sigma$ and (1,1) $B^1\Sigma \leftarrow\leftarrow X^1\Sigma$ transitions. Vibrational levels above $v'=1$ in the B-state predissociate on a time scale faster than the ionization rate. A pseudo ''two-point fit'' of the integrated line strengths gives a temperature, $T_{\text{vib}}=1100$ K; however, data are insufficient to assume any statistics. Only 6% of desorbing CO contains one quanta of vibrational energy.

encompasses only 7.5–10 cm^{-1} due to the similar rotational constants for the $v''=1$ and $v'=1$ states.

We find that for the $(2+1)$ REMPI detection scheme, the presence or lack of Q-branch structure is quite sensitive to probe-laser fluence and hence we have explicitly included a Lorentzian term in our simulation and fitting program to account for this intensity-dependent lifetime broadening.[36] We fit the measured rotational linewidths without constraining the Voigt profiles generated from the known laser bandwidth. Thus, the Doppler components within the rotational linewidths becomes a fitted parameter.

In addition, we independently make a cursory investigation of the angular distribution of desorbing CO at 295 K by rotating our sample with respect to the TOF detector and monitoring the $Q(J)=5$ rotational feature of $v=5$. The CO angular distribution indicates that the majority of CO desorption of anisotropic and is emitted within 20° of normal. Using this angular distribution of $\pm 20°$ and the fitted Doppler width of our rotational spectra, the most probable velocity of CO desorption normal to the crystal surface can be calculated and a temperature obtained. From the most probable velocity, a translational temperature of $T_{\text{trans}}=90\pm 20$ K is assigned. This corresponds well to the measured translational temperature in our TOF spectra and constitutes a second independent measurement of the desorbed CO velocity.

The parameters used to simulate the spectra of Fig. 5 are a temperature of $T=295$ K, a two-photon bandwidth (W_B) of 0.084 cm^{-1}, and a Doppler width (W_D) of 0.106 cm^{-1}. A total Gaussian width (W_G) is given by

$$W_G=\sqrt{W_D^2+W_B^2}.$$

From this it follows that $W_G=0.135$ cm^{-1}, which is effectively Doppler limited. The Lorentzian width, $W_L=0.02$ cm^{-1}, is consistent with the known lifetime of the B state although it is negligible relative to the precision of these calculations.

DISCUSSION

Experimental determination of the state resolved distribution of CO desorbed from calcite provides a detailed view of the product energy available in the photostimulated desorption process. It is usual for the products observed in most photostimulated desorption experiments to be emitted either thermalized or with a high translational energy, but in this work the photodesorbed CO is translationally cold. Subthermal desorption distributions are rare,[43] and we know of no reported case where the translational energy of desorbing molecules is as low as $\frac{1}{3}$ of the surface temperature. It seems unlikely that an equilibrium thermal desorption process could account for this phenomena. For example, one argument for ''cold'' thermal desorption would be that if energy equilibrium of an adsorbate with the surface occurs through small energy increments ($\ll kT$) the final small increment would then put the energy above the vacuum level, resulting in low translational motion. This implies a very steeply falling sticking probability with increasing temperature.[44] However, in our experiments this phenomenon appears pro-

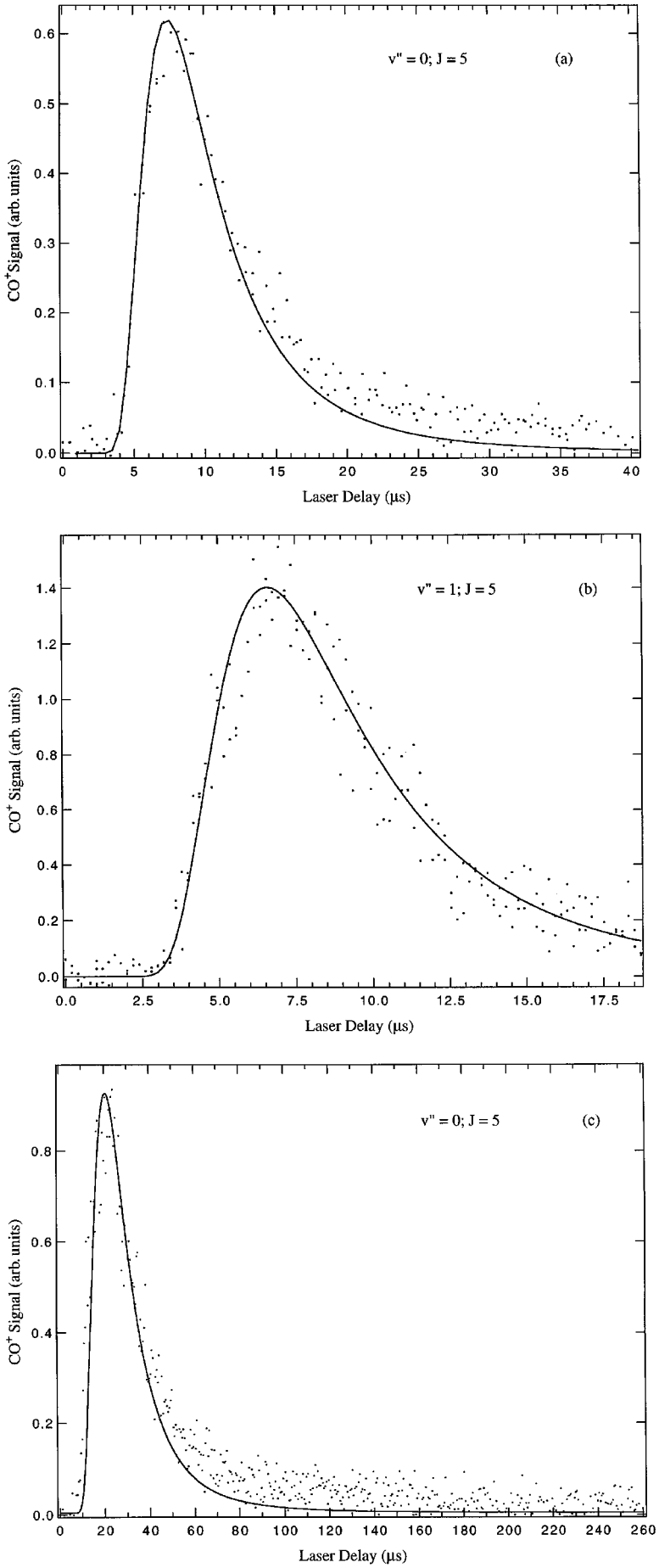

FIG. 4. Velocity dependence of CO desorbed from $CaCO_3$ monitored via $(2+1)$ REMPI of a $Q(5)$ transition at progressive laser delays. In (a) $v''=0$ can be fit to a translational temperature, $T_{\text{trans}}=110\pm15$ K, while in (b) $v''=1$ can be fit for $T_{\text{trans}}=125\pm15$ K using a half-range Maxwell-Boltzmann velocity distribution function (see text). These differences are within statistical error. In (c) the TOF spectra are displayed for $v''=0$ at a substrate temperature of 90 K. The fitted temperature of CO products, $T_{\text{trans}}=20\pm10$ K. At $t>60$ μs, the effective pumping rate of the chamber is considered in weighting TOF data.

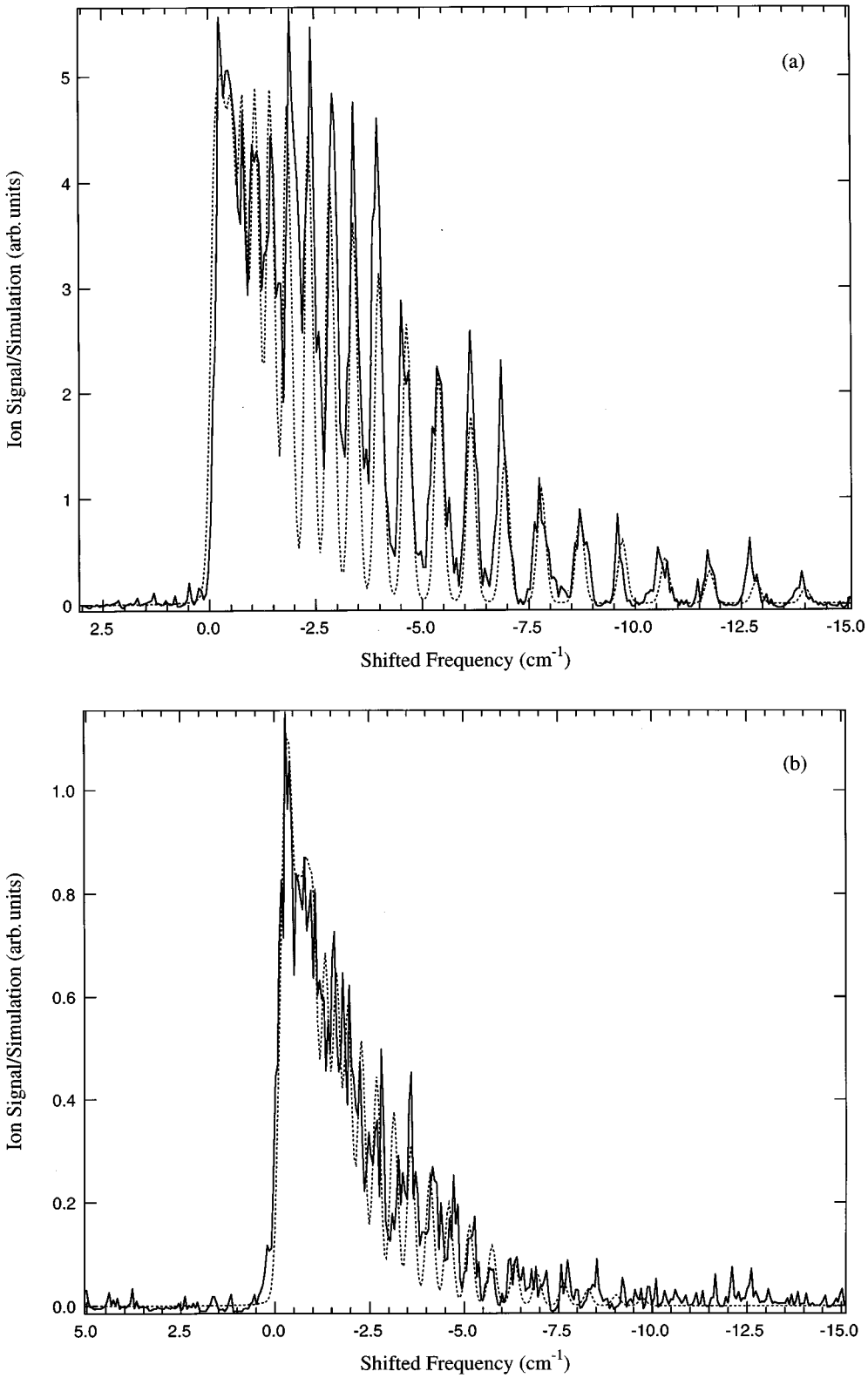

FIG. 5. Rotationally resolved Q-band spectra of desorbed CO. The $(2+1)$ REMPI scheme contains the entire Q band within a narrow frequency range of $<20\ \mathrm{cm}^{-1}$. (a) displays the spectrum for the CO (0,0) $B^1\Sigma \leftarrow\leftarrow X^1\Sigma$ transition. (b) displays the spectrum for the (1,1) $B^1\Sigma \leftarrow\leftarrow X^1\Sigma$ transition. Note here that predissociative transitions $Q(J)=16-18$ are observable indicating that for this scan the rate of ionization is greater than for the predissociation of these states. In all spectra, wavenumber incrementation runs progressively with the frequency scale shifted such that the $Q(J)=0$ transition is located at the band origin. The solid and dashed lines, again, represent the recorded spectra, and the simulated fits, respectively. The simulated fit is for a temperature of 295 K (see text).

nounced at $T=295$ K.[45,46] Similar arguments have been made by Higashi in a discussion of subthermal methyl radicals produced in 193-nm excimer laser desorption experiments on chemisorbed trimethyl aluminum.[43]

The intermediate species formed during the PSD of calcite are not known, and for now, the dynamics of CO formation are shrouded in the complexity of the surface dissociation. It is likely however, that the CO, once formed, does not stay near the surface long enough to exchange much energy with the surface. The low translational energy would then reflect the energetics of the CO formation. The nonthermal product distributions that we observe provide evidence that the product did not remain on the surface long enough to equilibrate. This likely indicates that a surface species or state is involved in the desorption process. The possible existence of a surface state in calcite, above 5 eV, has been

noted by Baer and Blanchard[25] and would suggest that excitations involving surface electronic states are involved. The processes that are clearly involved in the PSD of CO from calcite are photoexcitation and product desorption.

Photoexcitation

The photon energy relative to the material band gap is of paramount importance with regard to lifetime, mobility, and localization of the excitation. Due to uncertainties in the location of the calcite band gap (the estimated value $E_g = 6.0 \pm 0.35$ eV places the band gap at the high end of the error range for a 6.42-eV photon) either sub-band-gap or band-to-band excitation is feasible.[10,47] In fact, there is a high probability for direct absorption at the surface. Excitation could lead to the creation and mirgation of electron-hole pairs within the bulk, or at the surface, and could involve direct nonexciton mediated processes. The nature of bulk and surface excitons in calcite is unclear. Studies of thermoluminescence,[48–50] radioluminescence,[51,52] photoluminescence,[53,54] UV absorption,[54] and electron paramagnetic resonance (EPR) (Refs. 55 and 56) have been conducted of γ-ray and x-ray irradiated samples of natural carbonates which attempt to probe the nature of exciton formation and recombination. EPR studies found paramagnetic centers formed from self-trapped holes or electrons, such as CO_2^-,[57] CO_3^-,[56] and CO_3^{3-}.[56]

It is tempting to speculate that the electron-hole pair within calcite might then be described as an exciton associated with the electronic excited state CO_3^{2-}*. However, the most recent theoretical work[27] showing enhanced ''mixing'' of orbitals in the conduction-band region seems to indicate a more significant role for both Ca^{2+} and CO_3^{2-} in defining exciton character. The possibility exists that either excitons migrating from the bulk or that surface excitons created by direct absorption then dissociatively decay. These problems are related to our lack of information about the dissociation chemistry of this system, since CO_3^{2-} does not exist in the gas phase.

Product dissociation

In photostimulated desorption, it is expected that the translational motion is the degree of freedom most easily thermalized. Yet, the key feature of our results is the subthermal CO translational motion. This is inconsistent with the high translational energy associated with desorption from a dissociative surface excited state based on the conceptual picture in the Menzel-Gomer-Redhead (MGR) model.[58,59] The MGR model supposes that photoexcitation leads to formation of a ''molecular'' excited state significantly perturbed from its equilibrium position (analogous to an excited dissociative state of a gas phase molecule). The resulting lattice distortion then couples a significant fraction of the photon energy into nuclear motion and eventually into the translation of the atomic or molecular desorbate. Any such model that proposes the channeling of excess electronic energy into product translation necessarily predicts velocities much higher than we measure here. The model of Knotek and Feibelman[60,61] (KF) is widely invoked to explain the desorption of ionic species from insulating solids. This model proposes that like charge centers are formed in close proximity following an Auger electronic decay process. The Coulomb repulsion experienced by the nearby charged species then leads to the ejection of ionic centers at a high translational energy. While the concomitant ejection of neutral species, at somewhat lower velocities, is possible, we must reject the KF model, in the present case, on the grounds that the 6.4-eV photon is insufficient to induce any core excitation by a single-photon process.

Therefore, the qualitative dynamical picture that arises is one of a gentle reactive scattering; viewed as the *last half* of a full molecule/surface collision. Indeed, similar nonthermal rotational distributions—including rotational rainbows—have been observed in the full collision scattering of diatomic molecules off of metal surfaces [e.g., HD/P(111),[62,63] NO/Ag(111) (Refs. 64 and 65)]. It was observed that line strengths varied from one transition to another and underwent a nonlinear decline as the substrate temperature was increased (Debye-Waller effect). Noting that inelastic phonon energy transfer can account for 10–30 % of the collisional energy in diatom/surface interactions, Schinke and Gerber[66] elucidated this phenomena through a ''sudden'' approximation theory for thermal attenuation. Rapid scattering on a time scale faster than the nuclear motion of the molecule—coupled with an ''active'' surface involving phonon and diffraction effects—gives rise to final J levels which depend strongly on the phase (and eigenvalues) of the surface wave function and moderately on the incident scattering angle or orientation. On the other hand, the rotational distribution is perturbed from the surface temperature and seems to cut off at $Q(J) = 24$ (1180 cm^{-1}), which is within the dispersion range of the totally symmetric phonon mode of calcite centered at 1086 cm^{-1}.[67]

It is always necessary to consider the role of defect-driven processes in PSD and defect-driven molecular desorption of neutrals from calcium carbonate during ion bombardment and thermal decomposition under UHV conditions have been reported.[68,69] Baer and Blanchard observed neutral oxygen and carbon atoms as well as a 70% increase in CO_2 and a 40% increase in CO over background following electron-beam irradiation at 200 eV. In these studies, changes in the valence-band structure were observed and associated with the creation of surface defect sites.[25] Even the cleavage of calcite crystal results in the release of CO_2 and other species, often milliseconds after surface fracture by a defect-driven mechanism.[70] While a desorption pathway involving surface defects,

$$CaCO_3(s) \rightarrow CaO + CO_2(g) \tag{1}$$

can explain ion bombardment,[68,69] high-intensity CO_2 laser ablation,[71] and ESD (Ref. 69) results, it can not explain the present low fluence PSD results.

The delayed desorption of carbon dioxide following cleavage of calcite crystals is significant in that it is unambiguously related to massive lattice disordering at the surface and defect creation.[70] Since it is an extremely slow process, this delayed desorption will likely exhibit a final product state thermalized to the substrate temperature. We have tried to model such an occurrence for our CO desorption products from calcite, given their extremely low translational energy. No ''delayed'' thermal distribution at 295 K can be fit to our TOF data taken at room temperature, nor a thermal distribu-

tion of 90 K for our TOF data taken at that substrate temperature. We must conclude that the CO final products suffer no delay in their release from the surface and that the velocity distribution we measure in our experiments accurately reflects their translational energy.

It appears that a defect-driven desorption process from calcite includes (1) a predominant desorption product in the form of carbon dioxide, (2) desorbed products that often experience delayed release from the surface, and (3) an incubation period after which the desorption efficiency increases with time. While impurities and other sorts of defects are extant in geologic calcite, the nature of the product, the prompt release of CO, and the failure to observe either an incubation period or enhanced emission over time force us to reject the usual kinetic rate model for a surface defect-driven desorption process in this experiment.

CONCLUSIONS

The vibrational, rotational, and translational energy distribution of neutral CO formed following 193-nm laser excitation from air-cleaved calcite have been determined and we find low translational energy, non-Boltzmann rotational distributions, and a 6% population of the first vibrationally excited state. These product distributions are associated with an energy localization in the photodesorption process. We observe no incubation period followed by enhanced desorption in calcite, indicating that the usual model of surface defect-driven desorption is not the dominant process at work. Instead, we believe that the low kinetic energy and nonthermal internal motion of CO are associated with the prompt decay of a surface species or state. The photostimulated desorption of CO from calcite has prompted several projects. Theoretical calculations are underway to help elucidate the electronic structure of calcite. We are extending the present experimental study to different substrate temperatures, shorter wavelengths, and other desorption products.

ACKNOWLEDGMENTS

The authors were supported by the Divisions of Chemical Sciences of the Office of Basic Energy Sciences, U.S. Department of Energy and the Strategic Environmental Research and Development Program. Pacific Northwest National Laboratory is operated for the U.S. Department of Energy by Battelle under Contract No. DE-AC06-76RLO 1830. We are indebted to Professor Noriaki Itoh for his comments. We also thank Maureen McCarthy, Kristine German, Matt Sieger, Thom Orlando, and Professor Tom Dickinson for stimulating discussions.

*Corresponding author; Electronic address: wp_hess@pnl.gov

[1] K. H. Wedepohl, *Handbook of Geochemistry* (Springer-Verlag, Berlin, 1969), pp. 1–270.
[2] M. L. Alexander, M. R. Smith, D. Koppenaal, and J. Hartman (unpublished).
[3] R. A. Bradley, E. Lanzendorf, M. I. McCarthy, T. M. Orlando, and W. P. Hess, J. Phys. Chem. **99**, 11 715 (1995).
[4] J. C. Miller and D. B. Geohegan, in *Laser Ablation: Mechanisms and Applications-II*, edited by John C. Miller and David B. Geohegan, AIP Conf. Proc. No. 288 (AIP, New York, 1994).
[5] R. F. Haglund, Jr., M. Affatigato, and P. H. Bunton, in *Laser Ablation: Mechanisms and Applications-II* (Ref. 4), p. 26.
[6] P. H. Bunton, R. F. Haglund, Jr., D. Liu, and N. H. Tolk, Phys. Rev. B **45**, 4566 (1992).
[7] D. Liu, D. J. McClure, A. V. Barnes, R. G. Albridge, N. H. Tolk, and D. Russell, Phys. Rev. B **47**, 1553 (1993).
[8] V. E. Puchin and A. Shluger, Phys. Rev. B **49**, 11 364 (1994).
[9] V. E. Puchin, A. L. Shluger, K. Tanimura, and N. Itoh, Phys. Rev. B **47**, 6226 (1993).
[10] V. E. Puchin, A. L. Shluger, and N. Itoh, J. Phys. Condens. Matter **7**, L147 (1995).
[11] V. E. Puchin, A. L. Shluger, and N. Itoh, Phys. Rev. B **47**, 10 760 (1993).
[12] J. T. Dickinson, S. C. Langford, J.-J. Shin, and D. L. Doering, Phys. Rev. Lett. **73**, 2630 (1994).
[13] E. Matthias, H. B. Nielsen, J. Reif, A. Rosen, and E. Westin, J. Vac. Sci. Technol. B **5**, 1415 (1987).
[14] J. Reif, H. Fallgren, W. E. Cooke, and E. Matthias, Appl. Phys. Lett. **49**, 770 (1986).
[15] T. Kubo, A. Okano, J. Kanasaki, K. Ishikawa, Y. Nakai, and N. Itoh, Phys. Rev. B **49**, 4931 (1994).
[16] R. E. Walkup, P. Avouris, and A. P. Ghosh, Phys. Rev. Lett. **57**, 2227 (1986).
[17] R. E. Walkup, P. Avouris, and A. P. Ghosh, Phys. Rev. B **36**, 4577 (1987).
[18] R. E. Walkup, P. Avouris, and A. P. Ghosh, J. Vac. Sci. Technol. B **5**, 1423 (1987).
[19] H. Overeijnder, M. Szymonski, A. Haring, and A. E. De Vries, Radiat. Eff. **36**, 63 (1978).
[20] H. Overeijnder, M. Szymonski, A. Haring, and A. E. De Vries, Radiat. Eff. **38**, 21 (1978).
[21] H. Overeijnder, R. R. Tol, and A. E. DeVries, Surf. Sci. **90**, 265 (1979).
[22] D. R. Ermer, J.-J. Shin, S. C. Langford, K. W. Hipps, and J. T. Dickinson, J. Appl. Phys. **80**, 6452 (1996).
[23] J. T. Dickinson, J. J. Shin, and S. C. Langford, Appl. Surf. Sci. **96-98**, 326 (1996).
[24] K. Knutsen and T. M. Orlando, Phys. Rev. B (to be published).
[25] D. R. Baer and D. L. Blanchard, Jr., Appl. Surf. Sci. **72**, 295 (1993).
[26] A. J. Skinner, J. P. LaFemina, and H. J. F. Jansen, Am. Mineral. **79**, 205 (1994).
[27] K. M. Beck, M. I. McCarthy, and W. P. Hess, J. Electron. Mater. (to be published).
[28] T. Calderon, M. Aguilar, F. Jaque, and R. Coy-yll, J. Phys. C **17**, 2027 (1984).
[29] Y. Liang, D. R. Baer, I. M. McCoy, J. E. Amonette, and J. P. LaFemina, Geochim. Cosmochim. Acta **60**, 4883 (1996).
[30] R. I. Masel, *Principles of Adsorption and Reaction on Solid Surfaces* (Wiley, New York, 1996).
[31] G. W. Loge, J. J. Tiee, and F. B. Wampler, J. Chem. Phys. **79**, 196 (1986).
[32] L. F. DiMauro and T. A. Miller, Chem. Phys. Lett. **138**, 175 (1987).
[33] T. A. Spiglanin, R. A. Perry, and D. W. Chandler, J. Chem. Phys. **87**, 1568 (1987).
[34] P. J. H. Tjossem and K. C. Smyth, J. Chem. Phys. **91**, 2041 (1989).
[35] J. P. Looney, J. E. Harrington, K. C. Smyth, T. R. O'Brien, and T.

B. Lucatorto, J. Vac. Sci. Technol. A **11**, 3111 (1993).
[36] K. M. Beck, K. A. H. German, and W. P. Hess, Chem. Phys. Lett. **256**, 297 (1996).
[37] R. Webb, J. T. Dickinson and S. C. Langford, Nucl. Instrum. Methods Phys. Res. Sect. B **103**, 297 (1995).
[38] J. T. Dickinson (private communication).
[39] R. Kelly and R. W. Dreyfus, Surf. Sci. **198**, 263 (1988).
[40] R. W. Dreyfus, C. Phipps, and A. Vertes, in *Laser Ablation: Mechanisms and Applications-II* (Ref. 4), p. 285.
[41] K. P. Huber and G. Herzberg, *Constants of Diatomic Molecules* (Van Nostrand Reinhold, New York, 1979).
[42] M. Eidelsberg, J.-Y. Roncin, A. LeFloch, F. Launay, C. Letzelter, and J. Rostas, J. Mol. Spectrosc. **121**, 309 (1987).
[43] G. S. Higashi, J. Chem. Phys. **88**, 422 (1987).
[44] C. W. Muhlhausen, L. R. Williams, and J. C. Tully, J. Chem. Phys. **83**, 2594 (1985).
[45] J. C. Tully, Surf. Sci. **111**, 461 (1981).
[46] J. C. Tully (private communication).
[47] A. L. Shluger, L. N. Kantorovich, E. N. Heifets, E. K. Shidlovskaya, and R. W. Grimes, J. Phys. Condens. Matter **4**, 7417 (1992).
[48] F. W. Kolbe and A. Smakula, Phys. Rev. **124**, 1754 (1961).
[49] W. L. Medlin, Phys. Rev. **135**, 1770 (1964).
[50] W. L. Medlin, J. Phys. Chem. Solids **28**, 1725 (1967).
[51] M. Aguilar and M. I. Osendi, J. Lumin. **27**, 365 (1983).
[52] T. Calderon, M. Aguilar, and R. Coy-yll, Radiat. Eff. Lett. **76**, 187 (1983).
[53] V. A. Pedone, K. R. Certone, and R. C. Burruss, Chem. Geol. **88**, 183 (1990).
[54] T. Calderon, M. Aguilar, and R. Coy-yll, Thermochim. Acta **133**, 213 (1988).
[55] D. Lapraz and P. Iacconi, Phys. Status Solidi **36**, 603 (1976).
[56] S. A. Marshall, J. A. McMillan, and R. A. Serway, J. Chem. Phys. **48**, 5131 (1968).
[57] J. A. McMillan and S. A. Marshall, J. Chem. Phys. **48**, 467 (1968).
[58] D. Menzel and R. Gomer, J. Chem. Phys. **41**, 3311 (1964).
[59] P. A. Redhead, Can. J. Phys. **42**, 886 (1964).
[60] P. J. Feibelman and M. L. Knotek, Phys. Rev. B **18**, 6531 (1978).
[61] M. L. Knotek and P. J. Feibelman, Phys. Rev. Lett. **40**, 964 (1978).
[62] J. P. Cowin, C. F. Yu, and S. J. Sibener, J. Chem. Phys. **75**, 1033 (1981).
[63] J. P. Cowin, C. F. Yu, S. J. Sibener, and L. Wharton, J. Chem. Phys. **79**, 3537 (1983).
[64] G. D. Kubiak, J. E. Hurst, H. G. Rennagel, G. M. McClelland, and R. N. Zare, J. Chem. Phys. **79**, 5163 (1983).
[65] A. W. Kleyn, A. C. Luntz, and D. J. Auerbach, Surf. Sci. **117**, 33 (1982).
[66] R. Shinke and R. B. Gerber, J. Chem. Phys. **82**, 1567 (1985).
[67] P. J. Delfyett, R. Dorsinville, and R. R. Alfano, Phys. Rev. B **39**, 3845 (1989).
[68] D. R. Baer, D. L. Blanchard, Jr., M. H. Engelhard, and J. M. Zachara, Surf. Interface Anal. **17**, 1723 (1991).
[69] A. B. Christie, I. Sutherland, and J. M. Walls, Vacuum **31**, 513 (1981).
[70] J. T. Dickinson, L. C. Jensen, S. C. Langford, P. E. Rosenburg, and D. L. Blanchard, Jr., Phys. Chem. Miner. **18**, 320 (1991).
[71] A. Mansoor, T. DebRoy, and R. Roy, J. Am. Ceram. Soc. **73**, 733 (1990).